4.0 HAZARD ASSESSMENT RESULTS

4.1 SLOPE STABILITY (SOURCE AREAS 1–3)

For assessed source areas 1–3, the engineering geological cross-sections in Figure 13 were used as the basis of the numerical slope stability modelling. Geotechnical material strength parameters used in the modelling are from Tables 11 and 12. Models using variable shear strength parameters for the key materials were run to assess the sensitivity of the slope – along a given cross-section – to failure, and to take into account the on-going degradation of the rock mass in response to earthquake-induced fracturing.

Stability assessments were carried out adopting three different geotechnical material strength parameter models. Strength reduction was simulated by reducing the Geological Strength Index values to simulate the observed increased fracturing of the rock mass through the 2010/11 Canterbury earthquakes (Figure 19). The condition of the rock mass at the onset of the 2010/11 earthquakes was inferred from photographs of the cliff taken (by M. Yetton, Geotech Ltd.) immediately after the 4 September 2010 (Darfield) earthquake.

The parameters relating to the different models are presented in Table 17. All models were assessed using the current slope surface geometry, derived from the LiDAR survey 2011c.

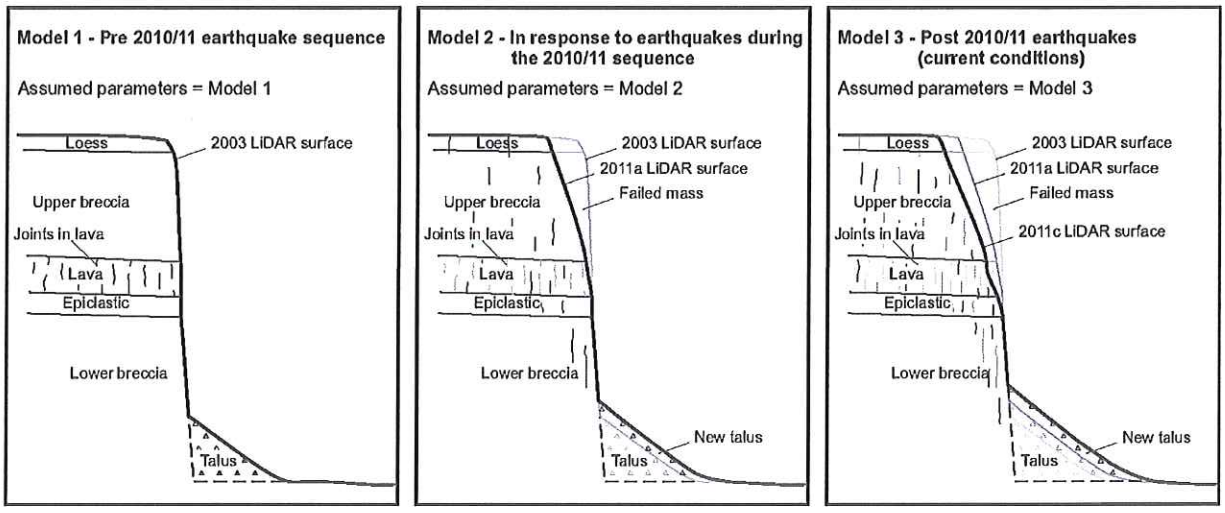

Figure 19 Schematic diagram showing the increasing frequency of defects in the slope in response to the successive 2010/11 Canterbury earthquakes.

Earthquake-induced cracks are unlikely to extend far back from the slope face near the toe of the slope, but are likely to extend further back from the slope face with increasing height from the toe. This is mainly because the amplification of shaking at the cliff crest is substantially greater than at the cliff toe.

Table 17 Material strength parameters used for modelling for cross-section 4 (similar parameters were adopted for sections 2 and 6, but the actual values used varied due to the different lithostatic stress range of the materials in the slope.

Model	Description	Earthquake	Material	Cohesion (c) (kPa)	Friction (ϕ) (degrees)
1	Average parameters (pre-22 February 2011 earthquake)	22 Feb 2011 13 Jun 2011	Loess Upper lava breccia Epiclastic Lava Lower lava breccia	10 100 190 1,650 250	30 31 47 69 26
2	Lower parameters (pre-13 June 2011 earthquake)	22 Feb 2011 13 Jun 2011	Loess Upper lava breccia Epiclastic Lava Lower lava breccia	10 70 130 670 160	30 23 38 68 14
1a	Average parameters, lava assumed to be breccia	22 Feb 2011 13 Jun 2011	Loess Upper lava breccia Epiclastic Lava (same as upper breccia) Lower lava breccia	10 100 190 100 250	30 31 47 31 26
2a	Lower parameters, lava assumed to be breccia	22 Feb 2011 13 Jun 2011	Loess Upper lava breccia Epiclastic Lava (same as upper breccia) Lower lava breccia	10 70 130 70 160	30 23 38 23 14
3	Post 2010/11 earthquakes (post 13 June 2011 earthquake)	22 Feb 2011 13 Jun 2011	Loess Upper lava breccia Epiclastic Lava Lower lava breccia	10 64 120 670 146	30 21 37 68 13

4.1.1 Slope stability – Static conditions (deep-seated failures)

Table 18 shows the results from the assessment, and graphic examples of stability assessment outputs are shown for cross-sections 2, 4 and 6 in Figure 20–Figure 22 for failures through the rock mass. Failures through the loess at the cliff crest and failure of the loess slumps (Figure 18) have not been modelled.

If a slope has a static factor of safety of one, then the slope is assessed as being unstable. Slopes relating to structures designed for civil engineering purposes are typically designed to achieve a long-term factor of safety of 1.5 under drained conditions, as set out in the New Zealand Building Code.

Results from the stability assessment indicate that under current conditions the factors of safety of the assessed cross-sections 2 and 4 are less than 1.5 adopting model 3 material parameters, and about 1.5–1.9 for cross-section 6.

Under current conditions it is possible that deep-seated failure of the rock mass for cross-sections 2 and 4 (adopting the assessed slide surfaces in Figure 20–Figure 22) could occur without an earthquake, given the relatively low factors of safety and sensitivity of the slope to surface water infilling tension cracks. However, it should be noted that material strengths – and therefore the slope factors of safety – could reduce with time, and the occurrence of future large earthquakes. It should also be noted that the stability assessment results presented are for deep-seated slide surfaces through the rock mass. However, much of the slope face appears unstable and rocks fall from the slope with no apparent trigger, indicating that parts of the slope face are only marginally stable to unstable, with factors of safety much less than those assessed for the deep-seated failures.

Table 18 Example results from slope stability assessment of source area 1 (cross-section 1).

Cross-section	Representative source area	Material strength parameter model (Table 17)	Tension crack condition	FoS[1] SLIDE	SRF[2] PHASE[2]	Pseudostatic yield acceleration (g)
2	2	1	Dry	2.3	-	-
		2	Dry	1.5	-	-
		3	Dry	1.4	1.6	0.3
		3	Filled	1.3	-	0.2
4	1	1	Dry	1.7		
		2	Dry	1.2		
		3	Dry	1.1	1.0	0.1
		3	Filled	1.0		<0.1
6	3	1	Dry	2.8		
		2	Dry	2.1		
		3	Dry	1.9	1.9	0.5
		3	Filled	1.5		0.4

Note: In the modelling, the role of defects on the stability of the rock mass have been taken into account by reducing the intact strength of the rock using the Geological Strength Index, therefore the modelling assumes the different units to be homogenous. The given factors of safety represent the overall stability of the larger slope for those slide surfaces shown in Figure 20–Figure 22. They do not represent the localised stability of each potential area or rock-block that could fall from the slope, as such failures are on-going.

[1] FoS is the factor of safety derived using the General Limit Equilibrium method of Morgenstern and Price (1965).

[2] The finite element model was also used for comparison. Where the slope has been assessed using the finite element model, the stability of the slope is assessed in terms of the stress reduction factor Note the shear strength reduction method is used to determine the Stress Reduction Factor (SRF) or factor of safety value that brings a slope to the verge of failure (Dawson et al., 1999).

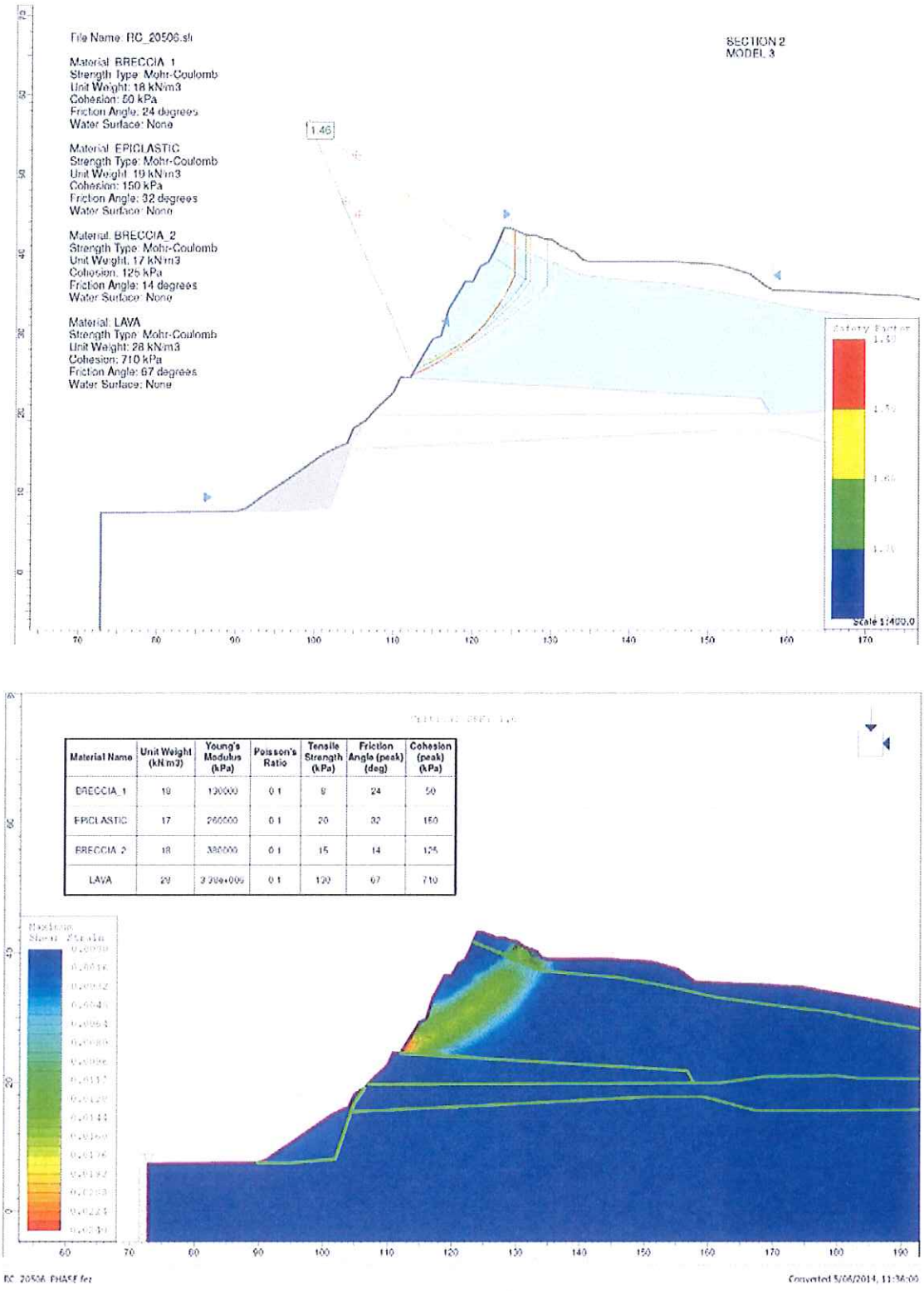

Figure 20 Example of limit equilibrium and finite element modelling results for cross-section 2 representing assessed source area 2, and adopting model 3 material parameters.

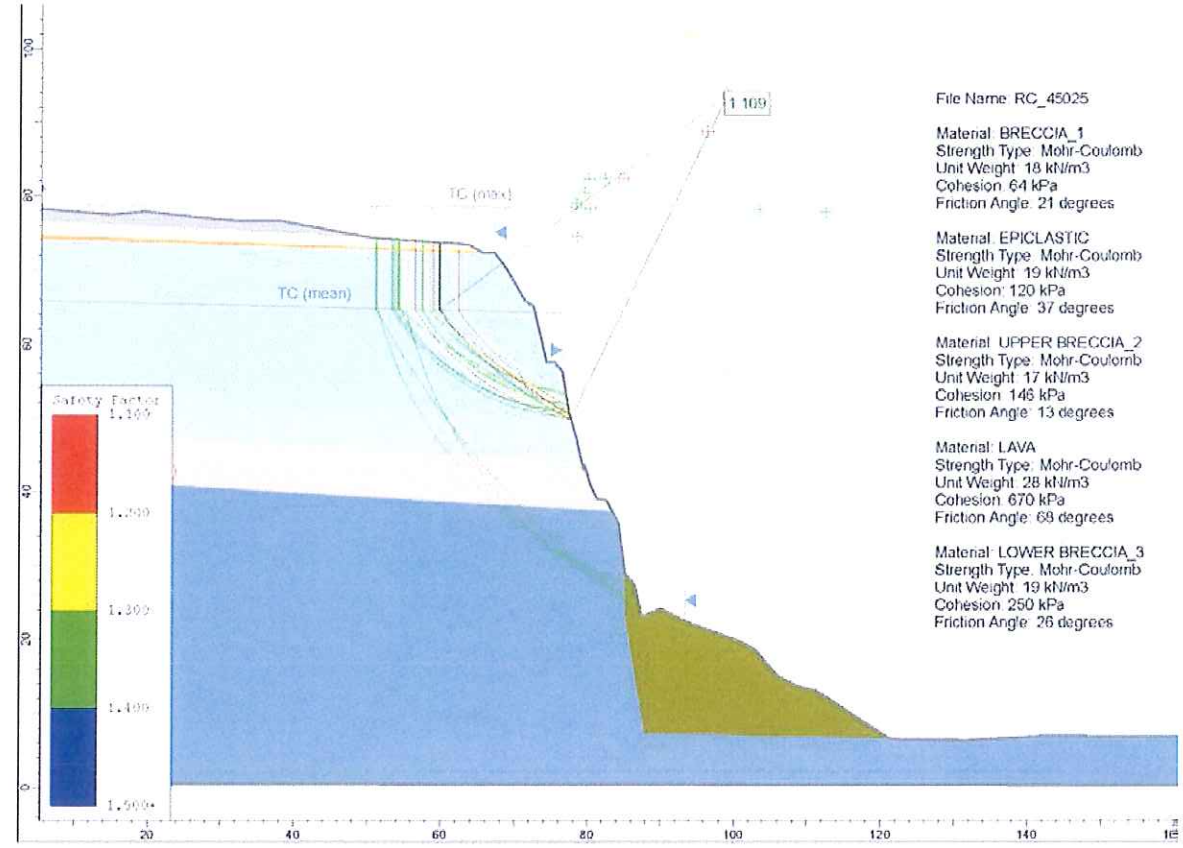

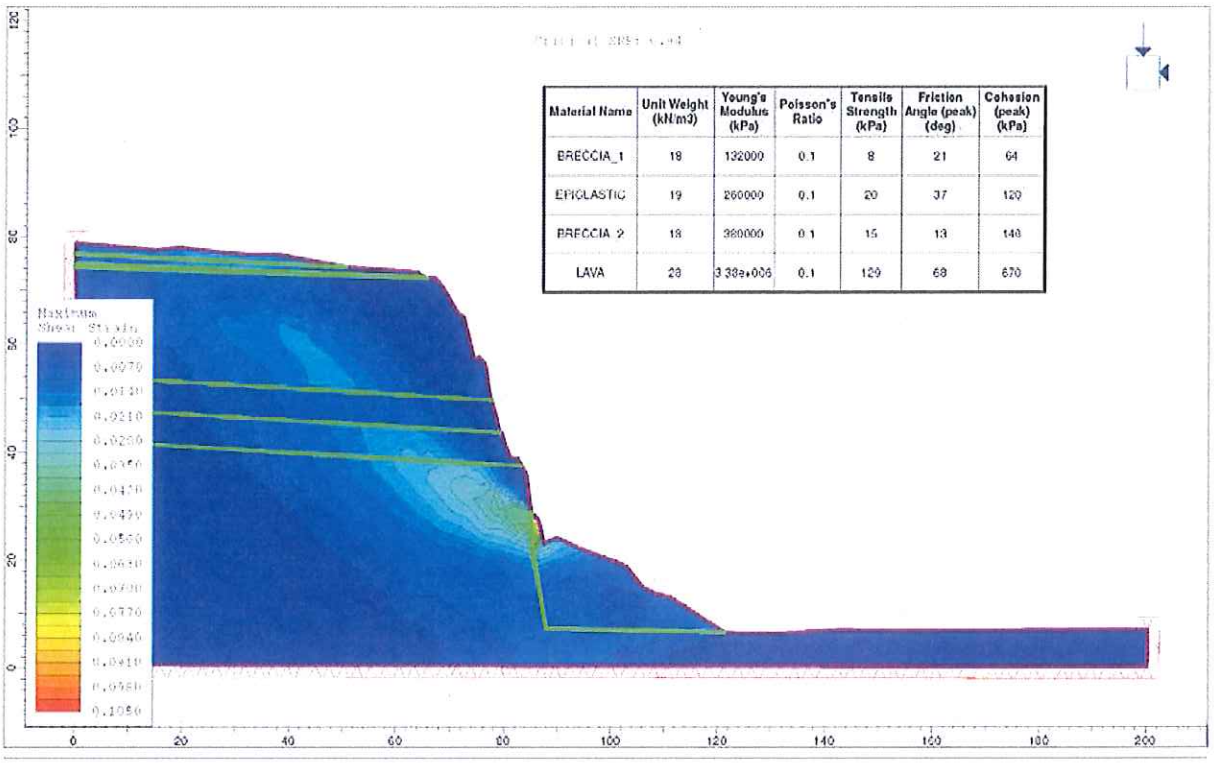

Material Name	Unit Weight (kN/m3)	Young's Modulus (kPa)	Poisson's Ratio	Tensile Strength (kPa)	Friction Angle (peak) (deg)	Cohesion (peak) (kPa)
BRECCIA_1	18	132000	0.1	8	21	64
EPICLASTIC	19	260000	0.1	20	37	120
BRECCIA_2	18	380000	0.1	15	13	146
LAVA	28	3.38e+006	0.1	129	68	670

Figure 21 Example of limit equilibrium and finite element modelling results for cross-section 4, representing assessed source area 1, and adopting model 3 material parameters.

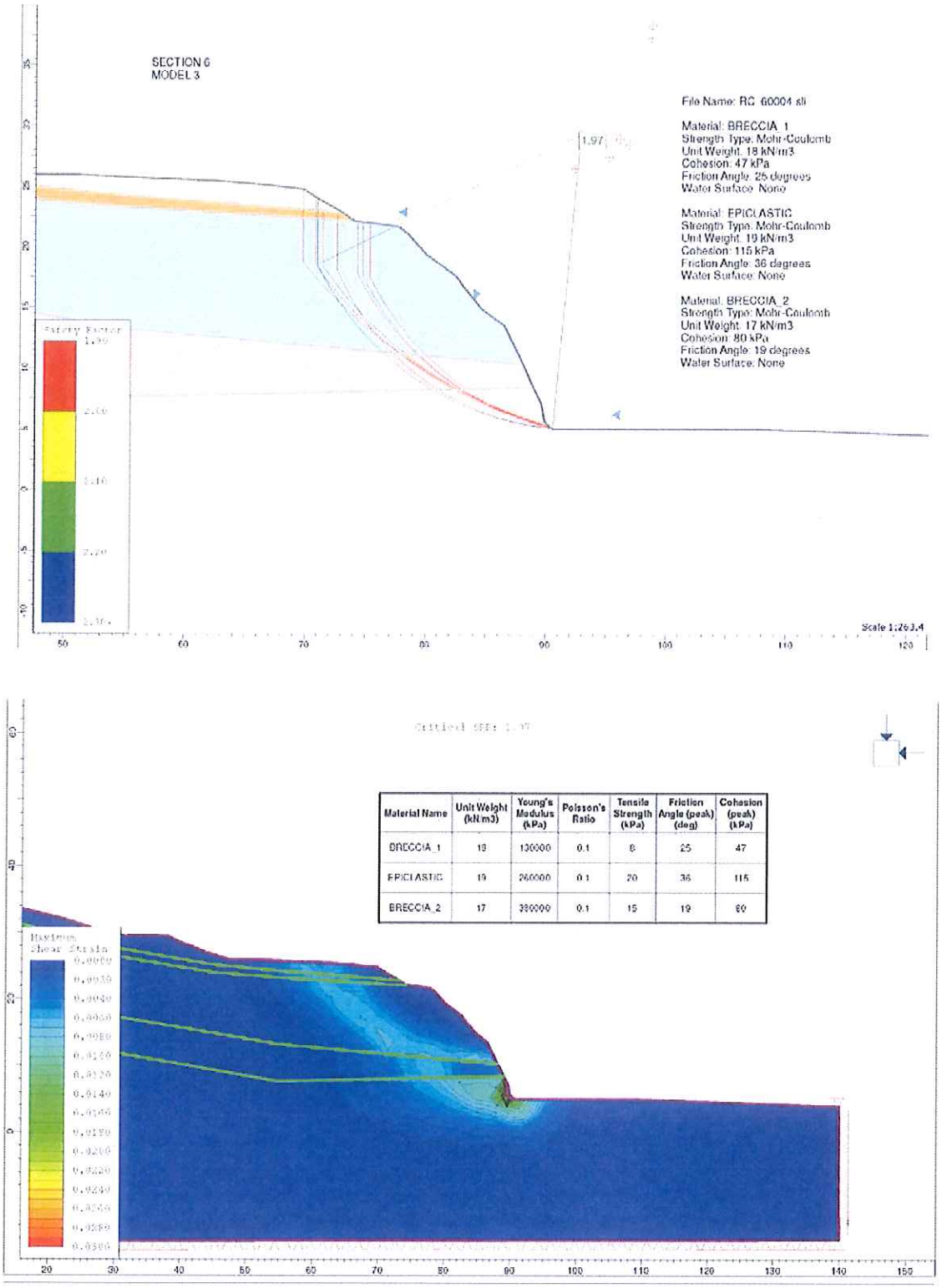

Figure 22 Example of limit equilibrium and finite element modelling results for cross-section 6, representing assessed source area 3, and adopting model 3 material parameters.

4.1.1.1 Model sensitivity to groundwater

The sensitivity of the slope factor of safety to transient changes in ephemeral ground water (pore pressure) has been simulated by modelling pore pressures acting within tension cracks, where the tension cracks are assumed to extend from the surface to the base of the basalt lava. Results are shown in Table 18.

The results show that the inclusion of water filled tension cracks within the model decreases the factor of safety for all cross-sections by 7–21%. The largest decrease is for cross-section 6. It should be noted that the stability model (Slide) used for modelling, can only model one water-filled tension crack. In reality there would be many water-filled tensions cracks and so these results do not fully reflect the impact of water filled tension cracks on slope stability.

4.1.1.2 Model sensitivity to slope geometry

The sensitivity of the slope factor of safety to changes in the slope geometry was assessed by adopting the different slope-surface geometries from the LiDAR surveys for cross-sections 2, 4 and 6, where material from the cliff fell off during the 2010/11 earthquakes, causing the slope geometry to change.

Results show that as material falls from the cliffs the factors of safety increase slightly as the slope angles reduce. Typically the increase in the factor of safety, for cross-sections 2, 4 and 6, is 5–10% between the slope geometries derived from the 2011a and 2011c LiDAR surveys, assuming material parameters are kept constant. However, any increase in stability caused by reducing slope angles, may be counterbalanced by fracture-induced weakening of the rock mass.

4.1.2 Slope stability – Dynamic conditions

Dynamic stability assessment comprised: 1) back-analysing the performance of the slope during the 2010/11 Canterbury earthquakes to calibrate the models and check that the calculated displacements were consistent with the displacements inferred during the earthquakes; and 2) using the calibrated models to forecast the likely magnitudes of future displacements under given levels of peak ground acceleration.

Cross-section 4 (representing assessed source area 1) has been assessed under dynamic conditions, assuming a drained slope, using the decoupled method. The likely yield accelerations for cross-sections 2 and 6 (representing source areas 2 and 3) were assessed using the pseudostatic method.

4.1.2.1 Amplification of ground shaking

The first stage of the assessment was to calculate the maximum acceleration at the slope crest (A_{MAX}) to quantify amplification effects caused by topography and or contrasting materials. The slope crest is defined as the convex break in slope between the lower steeper slope and the upper less steep slope. Results from the dynamic site response assessment are contained in Appendix 6.

Results from this assessment suggest that modelled peak acceleration at the slope crest (A_{MAX}) varies approximately linearly with the peak ground acceleration of the free-field input motion (A_{FF}) for the horizontal motion component, but non-linearly for the vertical motion component. The relationship between horizontal and vertical component values of A_{MAX} is strongly non-linear. Over the range of modelled peak horizontal accelerations, the peak

ground acceleration amplification factor (S_T) for cross-section 4 is about 2.6 (±0.1) for horizontal motions and 3.3 (±0.3) for vertical motions, times the input free-field peak accelerations. The input peak accelerations are those derived from the out-of-phase synthetic free-field rock outcrop earthquake time acceleration histories described by Holden et al. (2014).

The results suggest that the modelled ground accelerations increase with increasing height above the toe of the slope, but that the peak horizontal accelerations (for all modelled earthquakes) concentrate around the convex break in slope, defined as A_{MAX}.

4.1.2.2 Back-analysis of permanent slope deformation

Earthquake-induced permanent displacements were calculated using the decoupled method (Makdisi and Seed, 1978) and the Slope/W software. The failure mechanism assessed was failure of the slope through the rock mass. A range of slide surfaces were assessed adopting the "block search" and "semi-circular" functions. Permanent displacements was estimated along each slide surface, where the displacing mass was treated as a rigid-plastic body and no internal plastic deformation of the mass was accounted for, and the mass accrued no displacement at accelerations below the yield acceleration.

The out-of-phase synthetic rock outcrop earthquake time acceleration histories from the 22 February and 13 June 2011 earthquakes were used as inputs for the modelling, as permanent coseismic displacement of the Redcliffs slopes were inferred during these events, and large volumes of materials fell from the slopes. Variable material strength parameters were used for the main materials present, adopting model parameters 1–3 (Table 17).

For these assessments, the displacements inferred from crack apertures are assumed to represent the coseismic permanent displacement of the slope, along cross-section 1, during the 22 February, 13 June and 23 December 2011 earthquakes. The results from each modelled scenario were then compared to the inferred coseismic permanent slope displacements for each earthquake.

For the assessments the slope surface at the time of the earthquake was used adopting the LiDAR survey data. For example, back-analysis of the 22 February 2011 earthquake, uses the slope surface from the 2003 LiDAR survey, and back-analysis of the 13 June 2011 earthquake uses the 2011a LiDAR survey. All forecast modelling uses the 2011c LiDAR slope surface model.

The results from the modelling of the 22 February and 13 June 2011 earthquakes, adopting the parameters listed in Table 17, are summarised in Table 19. Figure 23–Figure 25 show the results for the different models.